Sensors and Materials, Vol. 34, No. 10 (2022) 3797–3812
MYU Tokyo

S & M 3077

Mechatronic Model of Tool Center Point for Evaluating Dynamic Behaviors for Machine Tools

Ben-Fong Yu,[1] Jenq-Shyong Chen,[2*] and Hung-Yih Tsai[3]

[1]Graduate Institute of Precision Manufacturing, National Chin-Yi University of Technology,
No. 57, Sec. 2, Zhongshan Rd., Taiping Dist., Taichung City 411030, Taiwan (R.O.C.)
[2]Department of Mechanical Engineering, National Chung Hsing University,
No. 145, Xingda Rd., South Dist., Taichung City 402202, Taiwan (R.O.C.)
[3]Department of Vehicle Engineering, National Formosa University,
No. 64, Wenhua Rd., Huwei Township, Yunlin Country 632301, Taiwan, (R.O.C.)

(Received May 26, 2022; accepted October 11, 2022)

Keywords: tool center point, mechatronic model, dynamic behavior, machine tool structure

In this study, we constructed the mechatronic model of a tool center point (TCP-MM) present in the virtual environment. Since the dynamic behavior of a TCP affects the productivity, geometric accuracy, and surface quality of machining parts, a TCP-MM can evaluate the dynamic behaviors of the motion trajectory. The TCP-MM of machine tools consists of the servo feed drive model inside the servo loop and the machine tool structure model with the TCP outside the servo loop. Firstly, we developed TCP position measurement equipment that collects the relative displacement between the tool and the workpiece. Subsequently, the frequency response of the actual machine tool is measured by servo excitation for each axis, and the frequency response function is obtained using position detectors including a motor encoder, linear scale, and TCP device. Finally, the TCP-MM is estimated by the system identification method. The effectiveness of the TCP-MM is verified for a specified path, and the dynamic behavior of the TCP at four quadrantal points of a circular path is observed upon acceleration and deceleration in the motion trajectory. The results of an experiment and a simulation indicate that the TCP-MM can predict the TCP condition during the feed motion via the toolpath.

1. Introduction

Computer numerical control (CNC) machine tools are an excellent example of mechatronics in practice. In this study, we propose a mechatronic model (MM) through the tool center point (TCP) and use the model to estimate the TCP motion trajectory of the machine tool at a high feed motion. The TCP is the actual machining position. Therefore, a complete electromechanical system of the machine tool must include the dynamic behavior of the TCP. Machine tool design has recently been subject to static structure analysis and mechanism component selection. However, when high-feedrate motion is required, the TCP dynamic behavior of the machine tool affects the performance in the fabrication of parts. Therefore, the objective of this study was to

*Corresponding author: e-mail: MichaelChen@dragon.nchu.edu.tw
https://doi.org/10.18494/SAM4093

ISSN 0914-4935
https://myukk.org/

combine a servo feed drive system with a machine tool structure of the TCP to develop a TCP-MM. The mathematical model predicted the dynamic behavior characteristics of the toolpath, such as the machining time, geometric accuracy, and surface quality. The TCP-MM is a fundamental technology of single-machine intelligence in intelligent manufacturing.

The machining performance of a CNC machine tool is derived from the relative motion of the tool and workpiece. The TCP displacement is equivalent to the relative position between the tool and the workpiece. Taking a moving column five-axis machine tool as an example, the column module includes the *Y*-axis, swivel head, and spindle to clamp the tool. The column module is situated on the saddle on the *Z*-axis. When the column module moves rapidly along the *Z*-axis, the moving member induces an inertial load, leading to the structural deformation and displacement of the TCP.[1] When acceleration and deceleration (ACC/DEC) occur at the feed axis, the inertial load of the moving part generates vibration at a constant feedrate, which affects the geometric accuracy and surface quality of the part.[2] Reducing the feedrate is an effective strategy to reduce the effect of the inertial load on the TCP. The geometric accuracy and surface quality of parts can thus be improved. However, the machining time is prolonged and the manufacturing efficiency is reduced.

The common sensors used for TCP displacement measurement include position gauges and accelerometers. Bringmann and Maglie proposed three linear probes for measuring the displacement of a TCP.[3] The dynamic response of three dimensions can be measured simultaneously, but the displacement of three axes must be calculated from measurement data from three linear probes. Owing to the limitation of the contact type, the moving range of the test path was limited and the dynamic behavior of the TCP might be insufficient. Lee *et al.*[4] and Nagaoka and Matsubara[5] used a cross grid encoder (KGM) for TCP measurement. Since the KGM performs noncontact optical measurement, it is suitable for dynamic tests in 2D contouring paths. More importantly, it is characterized by high-speed motion (80 mm/min), a wide measurement range (0.1–115 mm), and high accuracy (resolution as high as 1 nm). However, a KGM is expensive and difficult to install. Furthermore, as the optical mirror surface is likely to be damaged, it must be operated and maintained carefully. Hence, it is not practical for industry. In some studies, TCP displacement was observed through an accelerometer.[1,6–8] An accelerometer is usually used to measure vibration signals. It measures the signals of three dimensions simultaneously. It has a stable signal output, high sensitivity, quick response, and small size. These properties make it convenient to install on machine tools. Nonetheless, it has a human-induced installation error because the axial directions of the accelerometer and machine tool are not coincident. The position for each axis must be integrated from the relevant acceleration signal, which leads to the amplification of noise. Hence, in this paper, we propose a TCP device for TCP displacement measurement that performs noncontact optical measurement.

To enhance the performance of machine tools, many scholars have presented the MM of machine tools by system identification. Identification models were divided into two main classes: model-based models with physical significance and data-based models based on a data-driven method. The model-based models exhibit actual physical phenomena such as mechanical characteristics and the control system. These models mostly focus on the servo feed drive system inside the servo loop, including the servo-control loop and feed drive mechanism.[1,4,6,7,9–15] A

typical servo-control loop comprises current, velocity, and position loops. There is also semiclosed or fully closed loop control according to the position of the feedback. Many studies have defined the feed drive mechanism as two inertial systems.[6–7,9–11] The first inertial system contains the equivalent moment and damping from rotating members such as motor shafts, couplings, supporting bearings, and ball screws. The second inertial system is a second-order system that contains the equivalent "mass–spring–damper system". This system comprises linear moving parts such as slide tables, linear guideways, and nuts. In addition to proposing the MM, some studies discussed the input signal during system identification.[10] Some scholars focused on servo tuning via the MM according to the control method and used nonlinear identification mechanisms, for example, backlash and friction.[11–13] Lee *et al.* proposed a third inertial system that contains the equivalent mass–spring–damper system from the machine foundation.[4] Huang *et al.* and Liu *et al.* divided the rotating members of the first inertial system into the inertial system of a motor shaft and a fourth inertial system of rotating transmission mechanisms such as couplings, ball screws, and supporting bearings.[14,15] Dynamic characteristics such as the elastic deformation of a ball screw during feed motion can be discussed. A big data approach has been widely used in recent years. Many studies have proposed the MM of machine tools by a data-driven approach.[8,16–20] These studies presented models using neural networks based on input and output data. The MM can be constructed rapidly by data-driven identification. The accuracy of data-based models is increased and the variability is reduced by collecting a large amount of data from multiple machines with the same specifications. Some studies used optimization methods to improve the model precision, such as the genetic algorithm and particle swarm optimization. The output result was set as known and imported into the model for training, and the input parameters were optimized.[16,19] On the other hand, the output data was predicted by a model using the input data.[8,17,18] The data-based models are widely applied. The effects of the CNC parameters of the controller and the dynamic behavior of a TCP can also be considered.[8,16–18,20] The data-driven modeling approach is rapid, accurate, and applicable to machine tools produced in bulk. However, the data-based models have no physical significance. Undeveloped machine tool design or machine tool optimization strategies cannot be evaluated and planned, which is the main defect in data-driven modeling.

Numerous studies have aimed to develop an MM to optimize or improve the dynamic characteristics of mechatronics. Some studies focused on the toolpath planning of controller interpolation or the adjustment of servo control to enhance dynamic responses, while some discussed nonlinear characteristics. However, these studies presented the MM and research achievement based on the "motor encoder" or the "linear scale at the slide table". Nonetheless, the results obtained from these types of sensors cannot represent the actual tool cutting position.

In this study, we measured and modeled the mechatronic system of machine tools to obtain the dynamic behaviors of the TCP trajectory in high-feedrate motion. In Sect. 2, complete dynamic models of the TCP-MM are deduced, including the servo feed drive model inside the servo loop and the machine tool structure model with TCP dynamic characteristics outside the servo loop. The dynamic model of a system is displayed in a block diagram. The development of the TCP measuring equipment is discussed in Sect. 3. The frequency response of the feed drive mechanism and mechanical structure is measured by servo excitation. The system transfer

function is obtained by system identification and established in a digital environment. The advantage of TCP measurement is shown by a simple toolpath. The effectiveness of the TCP-MM is verified, and the dynamic behavior of the machine tool at a high feedrate is analyzed. Finally, a conclusion is provided in Sect. 4.

2. Deduction of TCP-MM

CNC machine tools are extensively used for manufacturing various parts. When a machine tool is operating during high-ACC/DEC feed motion, the axial thrust force has a greater effect on the machining performance than the cutting force. Figure 1 shows a servo motor applying thrust force (F_x) as the driving force. The servo feed drive system transfers the force via the carriage, bed, column, and headstock to the cutting point. The tool and workpiece generate relative displacement (X_{TCP}). In addition to the servo feed drive system inside the servo loop, a complete dynamic model must contain the dynamic characteristics of the TCP outside the servo loop.

2.1 Servo feed drive model

The conventional MM in the literature mostly focuses on the servo feed drive system in the servo loop. The system comprises servo-control loop and feed drive mechanisms. A typical servo-control system comprises a multilayer closed loop, as shown in Fig. 2. The innermost current loop drives the actuator, and the plant generates a response in the velocity loop from the instruction of the actuator. In this study, the plant is defined as the feed drive mechanism that implements the feed motion. The outermost position loop is fed back by the position sensor. To guarantee system stability, the controller of each loop is suitably adjusted. The common controllers of the servo loop of CNC machine tools mostly use a proportional (P)–integral (I) controller. In each loop, according to the difference between the input and output signals, the

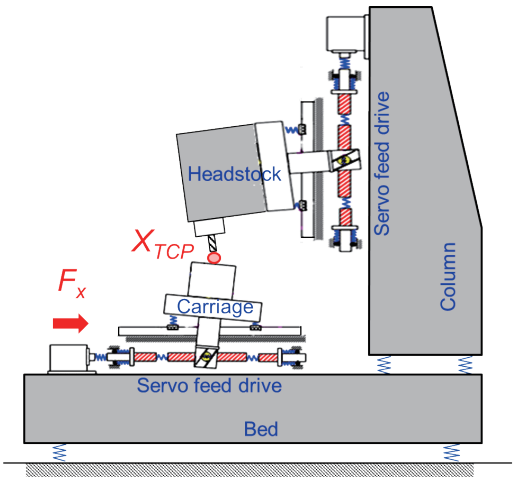

Fig. 1. (Color online) Schematic of dynamic behaviors with TCP.

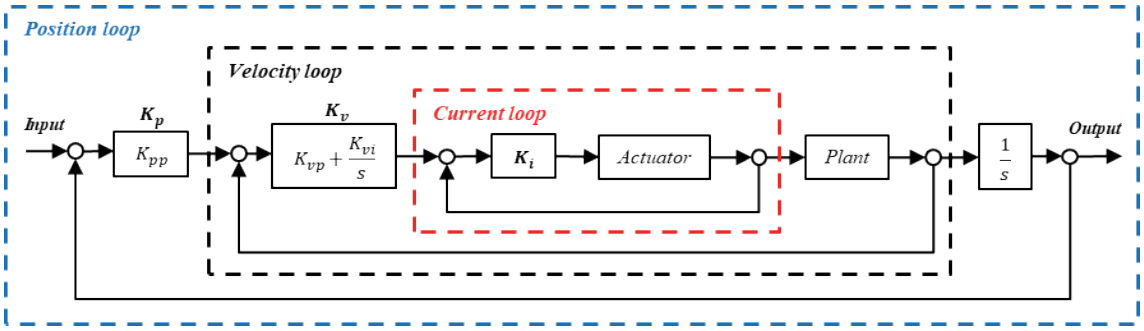

Fig. 2. (Color online) Typical servo-control system.

output signal is corrected by adjusting the PI controller so that the system responds accurately. A commercial driver that allows the user to set the current loop controller (K_i) is not available. On the other hand, the current loop has a larger bandwidth than the other loops. However, the excitation frequency is lower in machining that does not affect the stability of the current loop. Herein, K_i is set as 1. A velocity loop controller (K_v) is a PI controller, named as a velocity proportional gain (K_{vp}) and velocity integral gain (K_{vi}). A position loop controller (K_p) is usually a simple P controller, named as a position proportional gain (K_{pp}).

The dashed red frame in Fig. 3 contains a feed drive mechanism with the ball screw driven. The resonance of the feed drive mechanism induced by the servo motor has axial and torsional modes. In this study, we used four inertial systems to manifest the uniaxial feed drive mechanism: a motor shaft mechanism, rotating transmission mechanism, axial transmission mechanism, and bed mechanism. The motor shaft mechanism includes the inertia moment (J_m) and viscous friction coefficient (B_m) of the shaft. The rotating transmission mechanism comprises a ball screw, coupling, bearing, and traveling carriage. J_L is the equivalent inertia moment of the transmission system, B_L is the equivalent damping, K_L is the equivalent rotational stiffness, and R_L is the lead of the ball screw. The motor shaft and rotating transmission mechanisms are two inertial systems with torsional stiffness. The axial transmission mechanism is based on the axial stiffness from the rotating transmission mechanism with M_t, C_t, and K_t being the equivalent mass, equivalent damping, and equivalent stiffness of the axial transmission mechanism, respectively. The axial transmission mechanism can be regarded as the third inertial system. The fourth inertial system is the axial stiffness of the bed mechanism, including the equivalent mass M_b, equivalent damping C_b, equivalent stiffness K_b of the bed, foundational support, guideway, and bearing bracket.

We first analyzed the current loop and motor shaft mechanism of the servo feed drive model. The system input was the current command (i_c), and the output was the angular velocity of the motor (ω_m). In this study, the current controller was set to 1. Hence, i_c multiplied by the torque constant (K_{tc}) was the motor torque command (T_c). T_c was applied to the motor shaft mechanism, and the motor shaft was rotated. ω_m was obtained through the motor shaft mechanism, where ω_m is the velocity feedback signal of the velocity loop. The rotational angle of the motor ($\theta_m = \omega_m / s$) after the integration of ω_m was used as the input of the rotating transmission mechanism, where θ_m can be regarded as the displacement output of the motor shaft mechanism and was detected

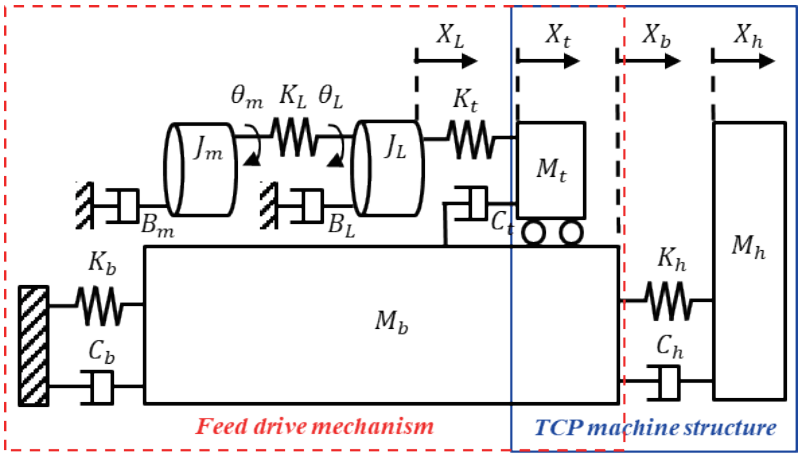

Fig. 3. (Color online) Lumped model representation with five inertial systems.

by the motor encoder. The angle difference ($\theta_m - \theta_L$) of the two rotatory inertias was multiplied by K_L to obtain the motor torque (T_m) of the driven rotating transmission mechanism, where the output was the rotation angle θ_L and the axial displacement was $X_L = \theta_L R_L$. Regarding T_m as the disturbance feedback applied to T_c, the transfer functions G_m and G_L of the motor shaft and rotating transmission mechanisms are respectively expressed as

$$G_m = \frac{\omega_m}{(i_c K_{tc} - T_m)} = \frac{1}{(J_m s + B_m)}, \tag{1}$$

$$G_L = \frac{\theta_L}{(T_m - F_t R_L)} = \frac{1}{(J_L s^2 + B_L s)}, \tag{2}$$

where $(\theta_m - \theta_L)K_L = T_m$. The position deviation ($X_L - X_{LS}$) between the rotating transmission mechanism and the linear scale of the carriage was multiplied by K_t to obtain the axial driving force (F_t). F_t was the input of the axial transmission mechanism (M_t and C_t) and bed mechanism (M_b, C_b, and K_b), from which the bed position (X_b) and carriage position (X_t) were obtained. The linear scale ($X_{LS} = X_t - X_b$) was equivalent to the position of X_t relative to X_b, and X_{LS} was the position feedback of the position loop. Therefore, the transfer functions G_t and G_b of the axial transmission and bed mechanisms are respectively expressed as

$$G_t = \frac{X_t}{F_t} = \frac{1}{M_t s^2 + C_t s}, \tag{3}$$

$$G_b = \frac{X_b}{F_t} = \frac{-1}{M_b s^2 + C_b s + K_b}, \tag{4}$$

where $(X_L - X_{LS})K_t = F_t$. In the experimental machine in this study, the motor encoder and linear scale positions of the carriage can be observed simultaneously; thus, Eqs. (1)–(4) were rearranged. The transfer function of the four inertial systems of the feed drive mechanism was reduced to the motor model (G_M) and transmission mechanism model (G_T), where G_T consists of G_L, G_t, and G_b, and the transfer functions of the complete G_M and G_T are expressed as

$$G_M = \frac{\omega_m}{i_c} = \frac{G_{\mathrm{m}}K_{tc}s\left[1 + G_LK_tR_L^2 + G_LK_L + K_t\left(1 + G_LK_L\right)\left(G_t - G_b\right)\right]}{s + G_{\mathrm{m}}K_L + G_LK_Ls + G_LK_tR_L^2s + K_t\left(s + G_LK_Ls + G_{\mathrm{m}}K_L\right)\left(G_t - G_b\right)}, \tag{5}$$

$$G_T = \frac{X_{LS}}{\theta_m} = \frac{G_LK_LK_tR_L\left(G_t - G_b\right)}{1 + G_LK_tR_L^2 + K_t\left(G_t - G_b\right)}. \tag{6}$$

In addition to the feed drive mechanism, the complete servo feed drive system includes the velocity and position loops of the servo-control loop. The input of the velocity loop was the velocity command (ω_c). i_c was obtained after calculating K_{vp} and K_{vi} of K_v, and ω_m was exported from G_M as the feedback signal of the velocity loop. Therefore, the transfer function (G_v) of the velocity closed loop is

$$G_v = \frac{K_vG_M}{1 + K_vG_M} = \frac{\left(K_{vp} + K_{vi}/s\right)G_M}{1 + \left(K_{vp} + K_{vi}/s\right)G_M}. \tag{7}$$

Finally, the position loop was applied. The input was the position command (θ_c) after the toolpath planning. K_{pp} of the position controller was used to obtain ω_c for the velocity loop. The position feedback of the position loop is X_{LS}; thus, the transfer function (G_p) of the position closed loop is

$$G_p = \frac{K_{pp}G_vG_T/s}{1 + K_{pp}G_vG_T/\left(sR_L\right)}. \tag{8}$$

2.2 Machine tool structure model with TCP

The solid blue frame in Fig. 3 contains the machine tool structure of the TCP model. The dynamic characteristic is the position deviation of the TCP (X_{TCP}), which is induced by the axial driving force of the motor applied to the machine tool structure. X_{TCP} is equivalent to the position of X_t relative to the tool position (X_h). Therefore, the TCP model of the fifth inertial system includes a column, Z-axis servo feed drive system, headstock, and spindle. It is represented by a mass (M_h)–damping (C_h)–spring (K_h) second-order system in this study.

$$G_h = \frac{X_h}{F_t} = \frac{1}{M_hs^2 + C_hs + K_h} \tag{9}$$

The TCP model is located outside the closed loop of the servo feed drive system. The input of this system is the position feedback X_{LS} and the output of this system is X_{TCP}. Therefore, the transfer function (G_{tcp}) of the TCP model can be expressed as

$$G_{tcp} = \frac{G_t - G_h}{G_t - G_b}. \tag{10}$$

The servo-control loop architecture in Fig. 2 is combined with the feed drive mechanism and machine tool structure in Fig. 3. The system block diagram of the complete uniaxial TCP-MM is illustrated in Fig. 4. The TCP-MM developed in this study includes a position loop, velocity loop, motor model, transmission mechanical model, and TCP model. The system input of the TCP-MM is the position command of the toolpath, and the output includes the position feedback inside the servo loop and the TCP position outside the servo loop. Different output results can easily reveal the dynamic response of the servo feed drive system and the dynamic behaviors of the TCP machine tool structure.

3. Construction and Verification of TCP-MM

The experimental machine tool is a three-axis vertical CNC machine tool, including a bed, saddle, table, column, and headstock. The *X*/*Y*/*Z* stroke is 510/360/300 mm. A workpiece moves on two dimensions and is set on the table. The table is placed on the saddle along the *X*-axis motion, and the saddle is moved on the *Y*-axis motion. A machine bed contains the saddle and table. The column is situated on the bed, and the column contains the headstock and feed drive system of the *Z*-axis. Herein, the tool and spindle are installed on the headstock, which is situated on the *Z*-axis. The control system adopts a commercial controller (10MA, Syntec Technology Co., Ltd.). The three-axis motors employ a servo motor and driver (ASDA-A2 series, Delta Electronics, Inc.), and the motors are provided with encoders. Additionally, the three axes are provided with linear scales (LS100 series, Heidenhain GmbH) as the position feedback of the servo-control loop. In this study, a TCP measuring device is developed for system identification, and a swept signal is used as the input. At the same time, the linear scale, motor encoder, and TCP position of the machine tool are measured simultaneously. According to the different output frequency responses and the system block diagram of the TCP-MM shown in Fig. 4, the system

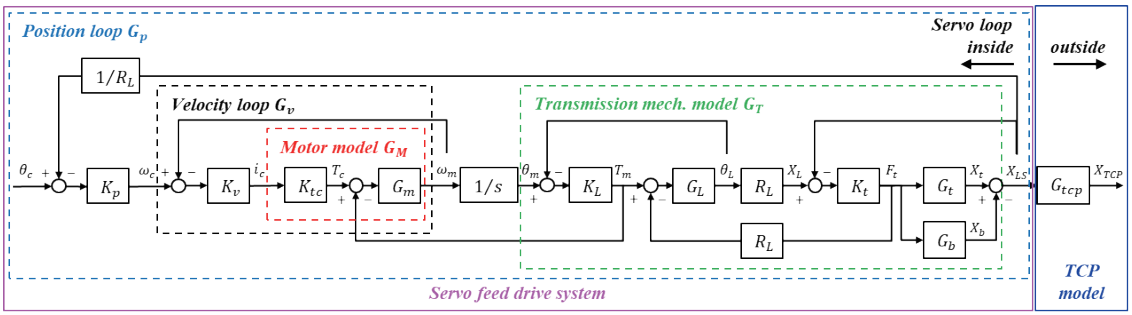

Fig. 4. (Color online) Block diagram of complete uniaxial TCP-MM.

transfer function of each axis is obtained by curve fitting. The actual TCP position is measured using a KGM, and the TCP position is predicted by simulation using the TCP-MM. The effectiveness of TCP modeling is verified via the 2D contouring path.

3.1 Development of TCP measuring equipment

The TCP is the actual machining position. When the machine tool is in high-ACC/DEC feed motion, the inertial load can affect the geometric accuracy and surface quality of the parts after machining. Therefore, in this study, we propose the use of the TCP-MM to predict the TCP displacement. First, simple and high-precision TCP measuring equipment was developed. The relative displacement of the tool and workpiece was measured, as shown in Fig. 5. A jig was designed for mounting the linear scale reader. The jig and reader were installed on the spindle by the tool holder, located close to the tool tip. Then, a high-stiffness fixture for mounting the linear scale body was designed to eliminate the effect of the accuracy of the TCP measurement in the high-ACC/DEC feed motion. The fixture and scale body were locked on the table in the orientation to be measured by approximating the workpiece machining position. The high-precision linear scale was a linear optical scale (Mercury 2000) produced by GSI MicroE Systems. The position signal output was in pulse form, and the resolution was as high as 0.078 μm. Table 1 shows a comparison of the resolutions of the position sensors. High-resolution and noncontact sensors can meet the requirements for measuring the dynamic characteristics of the TCP.

3.2 Construction of mathematical model of TCP-MM

To develop the TCP-MM for each axis, the digital model was estimated by system identification. Because K_{pp}, K_{vp}, and K_{vi} of commercial drivers can be regarded as known, the

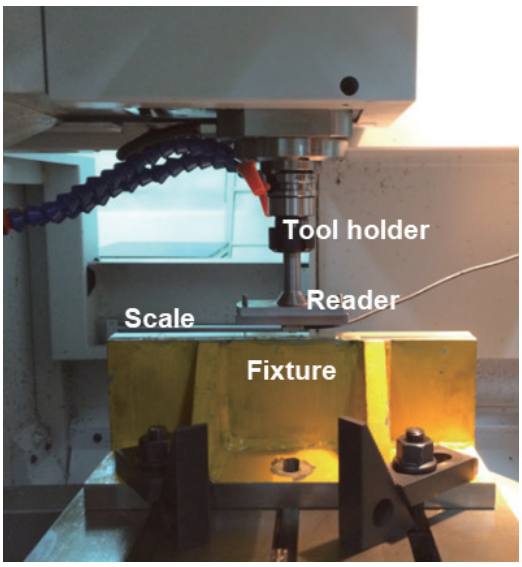

Fig. 5. (Color online) TCP measuring equipment.

Table 1
Comparison of resolutions of position sensors.

Device	Model	Resolution (μm/pulse)
Motor encoder	Delta, ASDA-A2	1.000
Linear scale	Heidenhain, LS100	1.000
High-precision linear scale	GSI MicroE Systems, Mercury 2000	0.078

most important task is to identify the system transfer functions of T_c to θ_m, X_{LS}, and X_{TCP}. A mathematical model was constructed as a system transfer function, as shown in Fig. 6. We used LabVIEW to generate a sinusoidal waveform as an excitation signal. The swept signal is used as the input. It is imported into the current command in the Delta driver, and the first output is obtained using the motor encoder. The motor drives the ball screw to move the table on the guideway, and the linear scale of the table is the second output. Finally, the dynamic response of the overall structure is excited. The third output is the high-precision linear scale at the TCP. The input and output signals are collected using the adapter card (NI, USB-6361). The time domain data of the experimental input and output signals [$u(t)$ and $y(t)$] are transformed by a fast Fourier transform (FFT) into $U(s)$ and $Y(s)$, respectively, in the frequency domain. The input frequency domain signal is divided by the output frequency domain signal to obtain the frequency response function (FRF) of the system, which is the system's dynamic behavior at various frequencies. The system FRF was combined with the system order derived in the previous section. The least squares method was used for curve fitting to estimate the system model. The square error of the differences between the fitted FRF and the actual FRF was used as the cost function, and the cost function was minimized iteratively. Finally, the system model was displayed as a mathematical model and regarded as the system's transfer function (system TF). The system TF was used to identify the transfer function of the mechanism, including the feed drive mechanism model inside the servo loop (G_M and G_T) and the TCP model outside the servo loop (G_{tcp}).

Figure 7 shows the three output signals, motor encoder, linear scale, and TCP, from top to bottom. For convenient observation and comparison, the rotation position of θ_m has been transformed into the linear position X_m. Figure 7(a) shows the results for the X-axis, where resonances occurred at about 3.0, 3.6, and 4.7 s; these resonances were observed in X_m but were not obvious. A resonance was clearly observed in X_{LS}, which was the third resonance at 4.7 s. The first resonance at 3.0 s was observed clearly only in X_{TCP}. Additionally, the resonances at 6.1 and 7.3 s were observed in X_{TCP} but not in X_m and X_{LS}. Figure 7(b) shows the results for the Y-axis, where clear resonances of Y_{TCP} occurred at 0.78, 2.7, and 6.3 s. Therefore, using the TCP to observe the dynamic response of the motor driving force is the most effective method to observe the low-frequency resonances of the machine tool structure.

Figures 8–10 show Bode plots of G_M, G_T, and G_{tcp}, respectively. The left and right figures represent the X and Y-axes, respectively. The solid blue line is the actual measurement result (Exp), whereas the red dashed line is the result of fitting after identification (ID). The input signal of G_M is i_c, the output signal is ω_m, and the mathematical model is shown as the system TF. Regarding the system TF G_T, the input signal is θ_m and the output signal is X_{LS}. The system TF G_{tcp}'s of the input and output signals are X_{LS} and X_{TCP}, respectively. Finally, the known servo parameter and system TF were substituted in Fig. 4 to obtain the TCP-MM for each axis. The

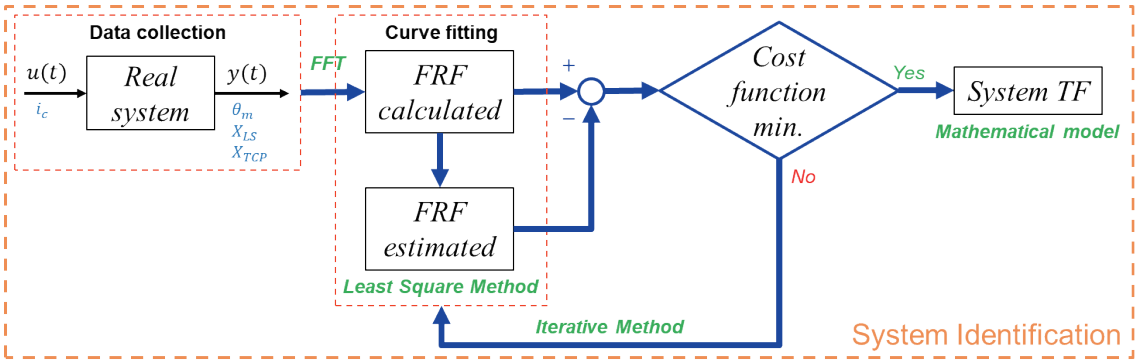

Fig. 6. (Color online) Mathematical model estimated by system identification.

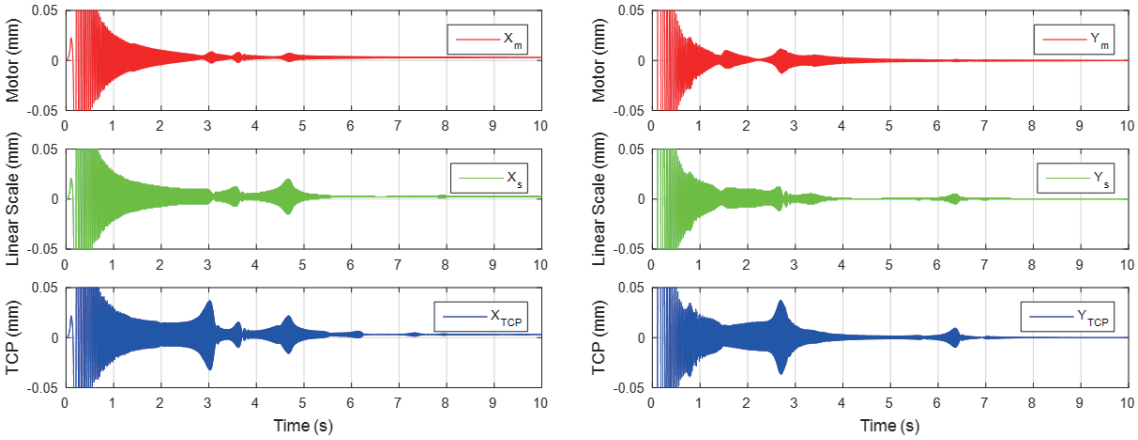

Fig. 7. (Color online) Experimental results of servo excitation in time domain.

digital version of the TCP-MM was executed in a MATLAB/Simulink environment as a block diagram including two servo loops and three mechanism models.

3.3 Verification of TCP-MM

We used a circular path on the *XY* plane with a radius of 35 mm and a feedrate of the NC code of 5000 mm/min to verify the TCP-MM. The toolpath included counterclockwise (CCW) and clockwise (CW) motions, respectively illustrated in Figs. 11(a) and 11(b). The black dashed line is the ideal path (Reference), the solid green line is the motor encoder (ENC), the red dotted line is the linear scale (LS), and the solid blue line is the TCP position measured using a KGM. An advantage of a circular path is that the contour error can be estimated easily. The greatest advantage of the circular motion is that it is synchronous motion in the *X*- and *Y*-axes, and there are axial ACC/DEC characteristics at four quadrantal point of the circle [Points A, B, C, and D in Fig. 11(a)]. For example, when the toolpath reaches Points B or D, the *X*-axis movement is

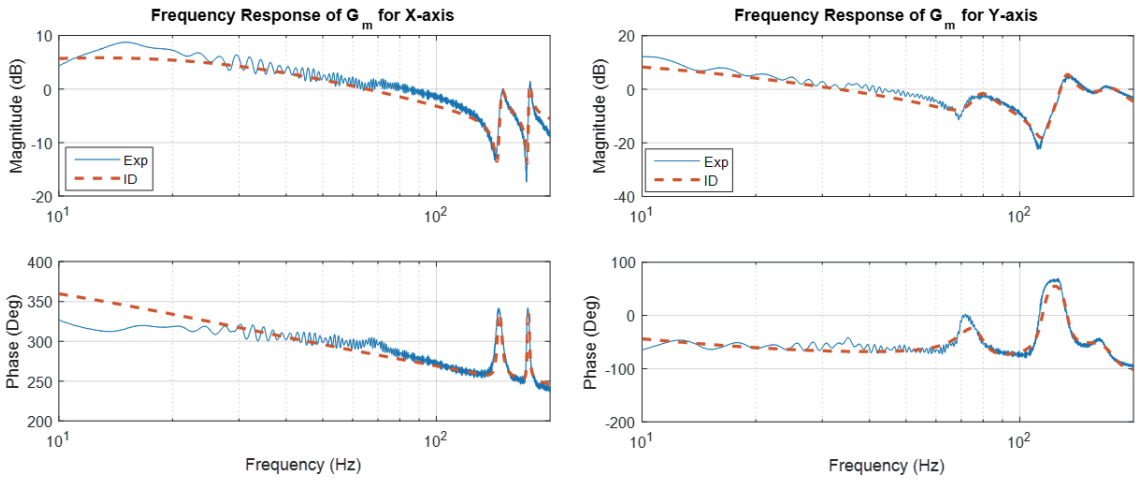

(a) (b)

Fig. 8. (Color online) Experimental FRF and system TF of G_M.

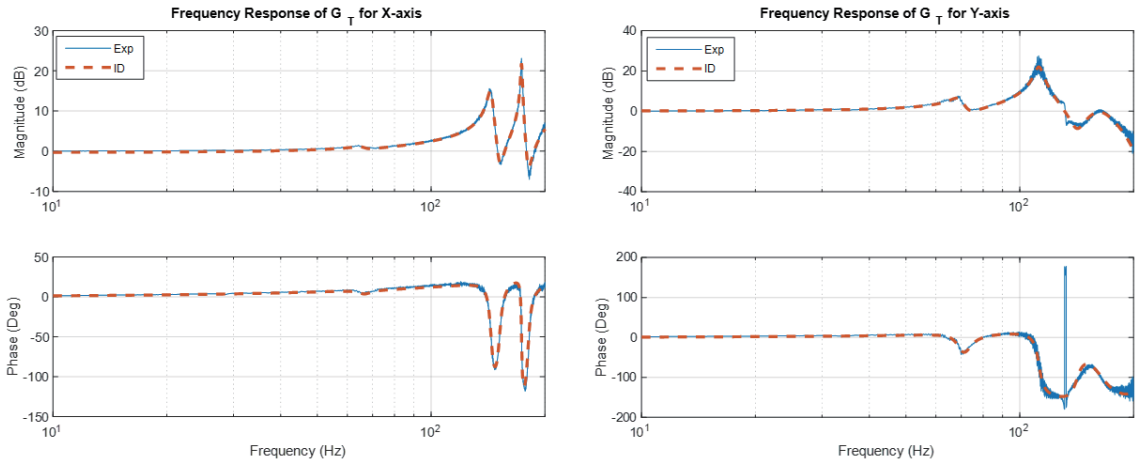

(a) (b)

Fig. 9. (Color online) Experimental FRF and system TF of G_T.

accelerated to the maximum feedrate and the *Y*-axis movement is simultaneously decelerated to zero. Subsequently, the *Y*-axis movement is immediately reversed to accelerate it, and the toolpath traverses Point B or D. The ACC/DEC motion excites the dynamic behavior of the machine tool. The reversal spike represents the effects of the mechanism backlash and friction. The oscillatory behavior after the *Y*-axis ACC/DEC of Point B/D is larger than that of the *X*-axis of Point A/C. This means that the *Y*-axis receives a larger inertial load in ACC/DEC feed motion. The experimental results demonstrated that the TCP could manifest the dynamic behavior of machine tools better than the motor encoder and linear scale. Subsequently, the interpolated position command was used as the input and the predicted TCP position (Sim-TCP with the

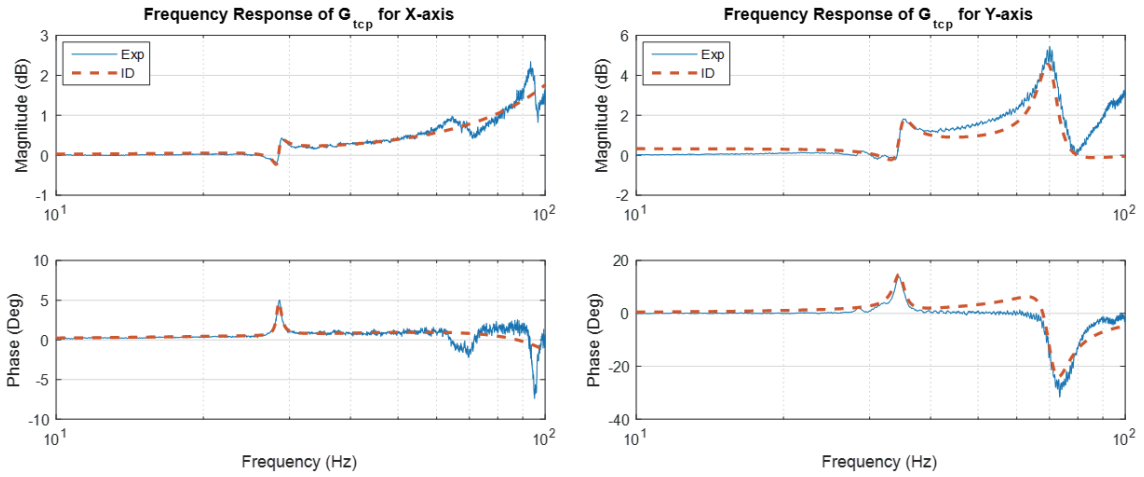

(a) (b)

Fig. 10. (Color online) Experimental FRF and system TF of G_{tcp}.

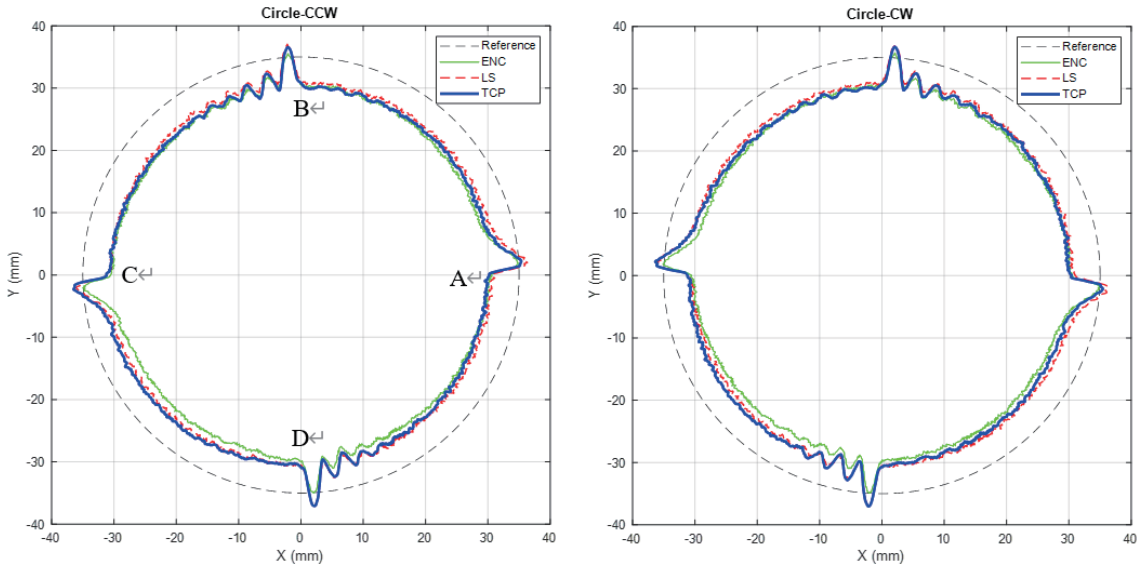

(a) (b)

Fig. 11. (Color online) Comparison of contour errors of three position sensors in CCW and CW trajectories.

dotted red line) was exported by the TCP-MM. The actual TCP position was measured using the KGM (Exp-TCP with the solid blue line), as shown in Fig. 12. The black dashed line is the ideal path (Reference). Table 2 shows the TCP verification results of the four reversal spikes and the contour error, which is used to obtain the difference between the TCP experiment and simulation. The differences of the four reversal spikes were 0.4–4.1 μm for the CCW trajectory and 0.7–3.8 μm for the CW trajectory. The differences of the contour errors in the CCW and CW trajectories

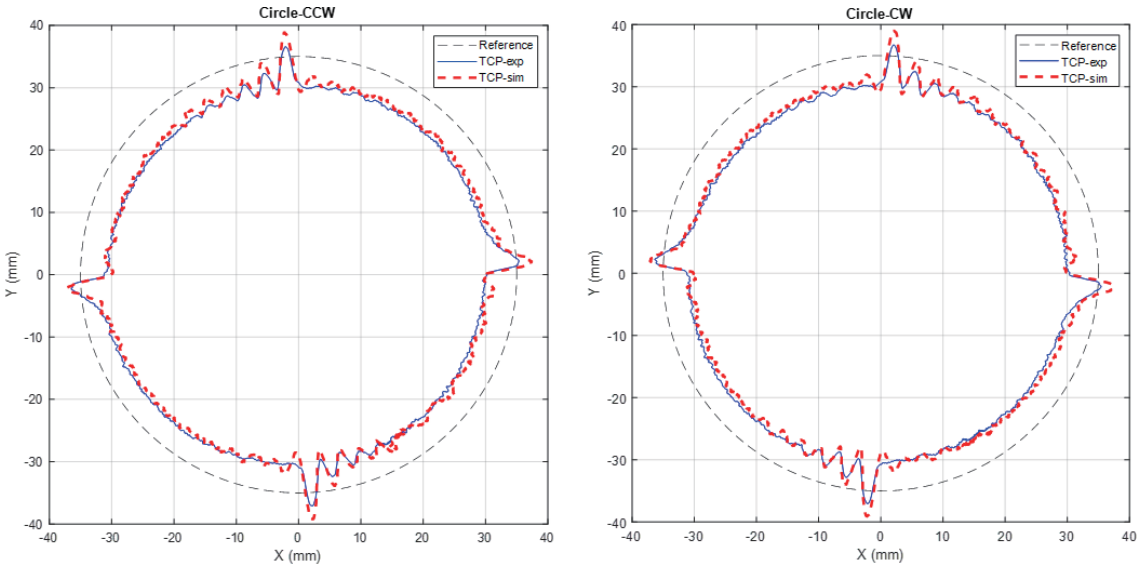

(a) (b)

Fig. 12. (Color online) Experimental and simulated results of circular path.

Table 2
Difference of TCP measurement and simulation.

Trajectory	Unit	Reversal spike at four quadrants				Contour error	Note
		A	B	C	D		
CCW	μm	0.4	2.5	3.0	4.1	0.6	Exp. – Sim.
CW	μm	0.7	2.6	2.2	3.8	0.6	Exp. – Sim.

were both 0.6 μm. The experimental results demonstrated that the TCP-MM could accurately predict the contour error and dynamic behavior of the circular path.

4. Conclusions

Machine tools are used to form a surface with the desired geometric characteristics by the relative motion of the tool and workpiece. We propose a mechatronic model of a machine tool based on the tool center point, named the TCP-MM. This model consists of a servo-control loop, the feed drive mechanism inside the servo loop, and the TCP machine tool structure outside the servo loop. This model has two servo-control loops, the position and velocity loops, and five inertial systems, the motor shaft mechanism, rotating transmission mechanism, axial transmission mechanism, bed mechanism, and TCP machine tool structure. First, to construct a complete TCP-MM, we developed TCP measuring equipment using a high-precision linear scale. A swept signal was imported into the servo feed drive system, and the output signals were collected using three types of position sensors: a motor encoder, table linear scale, and TCP measuring equipment. Various system transfer functions were estimated by system identification

from the input and output signals. Finally, the TCP-MM of various axes was set in a digital environment. The position command of a circular path was imported to predict the TCP dynamic behaviors such as the reversal spikes at the four quadrants of the circle and the oscillation occurring after ACC/DEC feed motion. The experimental results show that the motor encoder and linear scale in the ACC/DEC feed motion had the dynamic characteristics of four inertial systems. However, the TCP dynamic behavior was more significant. This means that the TCP machine tool structure of the fifth inertial system is indispensable to the MM. Regardless of the CCW or CW motion for the circular path, the differences of the TCP contour errors were the same (0.6 μm). Moreover, the simulated and measured TCP oscillation and vibration frequencies after ACC/DEC feed motion were coincident. Therefore, the proposed TCP-MM can successfully evaluate the TCP dynamic behavior through the trajectory motion.

Acknowledgments

This work was supported by the Ministry of Science and Technology, Taiwan (grant MOST 111-2222-E-167-001 – "Research on virtual mechatronic system and machining modes application based on tool center point of machine tools").

References

1 P. Parenti, G. Bianchi, N. Cau, P. Albertelli, and M. Monno: J. Mach. Eng. **11** (2011) 4.
2 B. Li, B. Luo, X. Mao, H. Cai, F. Peng, and H. Liu: Int. J. Mach. Tools Manuf. **72** (2013). https://doi.org/10.1016/j.ijmachtools.2013.06.004
3 B. Bringmann and P. Maglie: CIRP Ann. **58** (2009) 1. https://doi.org/10.1016/j.cirp.2009.03.104
4 K. Lee, S. Ibaraki, A. Matsubara, Y. Kakino, Y. Suzuki, S. Arai, and J. Braasch: In Laser Metrology and Machine Performance VI (WIT Press, Southampton, 2002).
5 K. Nagaoka and A. Matsubara: Proc. CIRP **1** (2012). https://doi.org/10.1016/j.procir.2012.05.007
6 M. Zatarain, I. Ruiz de Argandoña, A. Illarramendi, J. L. Azpeitia, and R. Bueno: CIRP Ann. **54** (2005) 1. http://dx.doi.org/10.1016%2FS0007-8506(07)60130-9
7 R. Sato, G. Tashiro, and K. Shirase: Int. J. Autom. Techol. **9** (2015) 6. https://doi.org/10.20965/ijat.2015.p0689
8 H.-C. Tseng, M.-S. Tsai, C.-C. Cheng, and C.-J. Li: Appl. Sci. **11** (2021) 4. https://doi.org/10.3390/app11041665
9 A. Matsubara, Y. Kakino, and Y. Watanabe: Proc. 2000 Japan*USA Flexible Automation Conf. (Michigan, 2000).
10 A. Casquero, R. Hecker, D. Vicente, and M. Flores: ABCM Symp. Series Mechatron. **4** (2010).
11 R. Sato: Key Eng. Mater. **516** (2012). https://doi.org/10.4028/www.scientific.net/KEM.516.154
12 C.-Y. Lin and C.-H. Lee: Appl. Sci. **7** (2017) 8. https://doi.org/10.3390/app7080776
13 K.-F. Lee and C.-H. Lee: Asian J. Control **22** (2020) 6. https://doi.org/10.1002/asjc.2292
14 H.-W. Huang, M.-S. Tsai, and Y.-C. Huang: Int. J. Mach. Tools Manuf. **132** (2018). https://doi.org/10.1016/j.ijmachtools.2018.05.002
15 C.-C. Liu, M.-S. Tsai, M.-Q. Hong, and P.-Y. Tang: J. Manuf. Mater. Process. **4** (2020) 1. https://doi.org/10.3390/jmmp4010021
16 W.-F. Kuo, and C.-H. Lee: 2019 Int. Conf. Engineering, Science, and Industrial Applications (ICESI) (2019). https://doi.org/10.1109/ICESI.2019.8862997
17 H.-W. Chiu and C.-H. Lee: IEEE Access **8** (2020) 51062. https://doi.org/10.1109/ACCESS.2020.2980286
18 B.-S. Chen and C.-H. Lee: Appl. Sci. **10** (2020) 10. https://doi.org/10.3390/app10103592
19 Y.-P. Liu and Y. Altintas: Precis. Eng. **73** (2022) 409. https://doi.org/10.1016/j.precisioneng.2021.10.010
20 A. Dietmair and A. Verl: Modern Mach. Sci. J. **3** (2009) 4. https://doi.org/10.17973/MMSJ.2009_10_20090604

About the Authors

Ben-Fong Yu received his B.S. and M.S. degrees from Da Yeh University and National Chung Cheng University, Taiwan, in 1999 and 2001, respectively, and his Ph.D. degree from National Chung Hsing University, Taiwan, in 2021. He worked in Goodway Machine Corp. and Ken Ichi Machine Co., Ltd., Taiwan, from 2002 to 2013 and 2017 to 2021, respectively. Since 2022, he has been an assistant professor at National Chin-Yi University of Technology. His research interests are in mechanical design, vibration, thermal issues, mechatronics, and intelligent technology in machine tools. (bfyu@ncut.edu.tw)

Jenq-Shyong Chen received his B.S. and M.S. degrees from National Cheng Kung University and National Taiwan University, Taiwan, in 1982 and 1984, respectively, and his Ph.D. degree from University of Michigan, USA, in 1991. From 1991 to 2010, he was a professor at National Chung Cheng University. Since 2010, he has been a professor at National Chung Hsing University. His research interests are in optical measurement, sensors, intelligent machine tools, laser precision machining, and ultrasonic machining. (MichaelChen@dragon.nchu.edu.tw)

Hung-Yih Tsai received his Ph.D. degree from National Chung Cheng University, Taiwan, in 2013. From 2013 to 2016, he was a postdoctoral researcher at National Chung Hsing University, Taiwan. From 2016 to 2019, he was a system integration assistant engineer and project leader at Automotive Research & Testing Center. Since 2019, he has been an assistant professor at National Formosa University. His research interests are in mechatronics systems, vehicle electronics engineering, automation control, and sensors. (hungyih@nfu.edu.tw)